Atmos. Chem. Phys. Discuss., https://doi.org/10.5194/acp-2018-796
Manuscript under review for journal Atmos. Chem. Phys.
Discussion started: 3 September 2018

Atmospheric Chemistry and Physics Discussions

Estimating vehicle carbon dioxide emissions from Boulder, Colorado using horizontal path-integrated column measurements

Eleanor M. Waxman[1], Kevin C. Cossel[1], Fabrizio Giorgetta[1], Gar-Wing Truong[1,2], William C. Swann[1], Ian Coddington[1], Nathan R. Newbury[1]

[1]Applied Physics Division, NIST Boulder
[2]Now at: Crystalline Mirror Solutions

Abstract

We performed seven and a half weeks of path-integrated concentration measurements of CO_2, CH_4, H_2O, and HDO over the city of Boulder, Colorado. An open-path dual-comb spectrometer simultaneously measured time-resolved data across a reference path, located near the mountains to the west of the city, and across an over-city path that intersected two-thirds of the city, including two major commuter arteries. By comparing the measured concentrations over the two paths when the wind is primarily out of the west, we observe daytime CO_2 enhancements over the city. We then use a Gaussian plume model to estimate city emissions of on-road CO_2 as $(6.9 \pm 1.8) \times 10^5$ metric tons (MT) CO_2/year, compared to the city bottom-up greenhouse gas inventory for the on-road vehicle sector of 4.5×10^5 MT CO_2/year. The two values nearly agree to within the quoted uncertainty, which does not include additional systematic uncertainty associated in the temporal and spatial scaling of the given measurements to annual city-wide emissions. Finally, we discuss experimental modifications that could lead to improved estimates.

1. Introduction

Measurements of greenhouse gases, especially CO_2 and CH_4, are critical for monitoring, verification, and reporting as countries and cities work towards decreasing their carbon emissions. Measurements on the city-scale are critical because cities contribute to a large fraction of global emissions (Marcotullio et al., 2013; Seto et al., 2014). However, quantification of city greenhouse gas emissions is challenging, especially for CO_2 since it has a high background and numerous point and diffuse sources including traffic, power plants, and animal and plant respiration. Emissions of pollutants are typically determined using two methods: top-down measurements over a specific site or area, and bottom-up inventories that calculate emissions based on sector activity and sector emissions factors. Significant work has been done recently to compare and reconcile these two methods for CH_4 emissions from oil and natural gas sources, e.g. (Allen, 2014; Zavala-Araiza et al., 2015) and for CO_2 in Indianapolis (Gurney et al., 2017) as well as ongoing work in Los Angeles (e.g. (Verhulst et al., 2017)), Paris (e.g. (Staufer et al., 2016)), and other cities through the Megacities Carbon Project.

Quantification of CO_2 fluxes from cities has primarily been determined from eddy covariance flux measurements with a point sensor located on a tower in or near a city, e.g. (Nemitz et al., 2002; Velasco et al., 2005; Coutts et al., 2007; Bergeron and Strachan, 2011; Velasco et al., 2014). However, for a single sensor, the relatively small footprint of the eddy covariance flux measurements limits the utility of this technique for large cities.

To overcome this limitation, tower networks of point sensors can measure CO_2 at multiple sites within a city and at background sites outside the city, e.g. (McKain et al., 2012; Lauvaux et al., 2013; Bréon et al., 2015; Staufer et al., 2016; Lauvaux et al., 2016; Shusterman et al., 2016; Mueller et al., 2017). To distinguish the small enhancements compared to the large background, these networks often use expensive, high-precision cavity ringdown (CRDS) instruments resulting in a high cost. The BEACO$_2$N network (Shusterman et al., 2016), on the other hand, has a much lower cost per sensor but requires

significant calibration for quantitative results. All of these methods use an inversion to determine the total emissions and thus rely heavily on well-known priors and high-resolution mesoscale atmospheric models.

More recently, several other approaches that do not rely as heavily on well-known priors have also been applied to city-scale emissions. Aircraft mass balance measurements (White et al., 1976; Ryerson et al., 2001) have been used to determine city emissions from Indianapolis (Mays et al., 2009; Heimburger et al., 2017) during the INFLUX campaign (Davis et al., 2017), following previous CH_4 emissions measurements from oil and gas fields (Karion et al., 2013, 2015). However, this method is costly and labor intensive, and therefore not suited to long-term continuous measurements. Column measurements from the Total Carbon Column Observation Network (TCCON) were used to calculate total South Coast Air Basin (SoCAB) CO and CH_4 emissions, but not CO_2 (Wunch et al., 2009). Satellite-based instruments have not yet quantified city CO_2 emissions, though OCO-2 may yield CO_2 emissions from megacities like Los Angeles, Riyadh, and the Pearl River Delta region (Ye et al., 2017), albeit with low temporal resolution with the current generation of satellites.

As an alternative to these approaches, horizontal, kilometer-scale, open-path instruments could in principle be used to determine CO_2 emissions from cities. Such instruments are capable of continuous measurements over a large area with a single instrument, e.g.(Wong et al., 2016; Dobler et al., 2017; Coburn et al., 2018). These sensors also have the advantage of being insensitive to small changes in local meteorology and are not subject to the same representation errors as point sensors (Ciais et al., 2010). Several such systems have been deployed. A laser absorption spectrometer system (GreenLITE) has mapped CO_2 concentrations over Paris, but has not yet been used to quantify emissions (Dobler et al., 2017). The California Laboratory of Atmospheric Remote Sensing Fourier Transform Spectrometer (CLARS-FTS) is a downward-looking slant column Fourier transform spectrometer (FTS) that scans across 28 measurement targets in the Los Angeles Basin to measure CO_2, CH_4, and O_2. Based on the measured CH_4:CO_2 ratio and the bottom-up CO_2 inventory from California Air Resources Board, researchers have calculated the LA Basin CH_4 emissions (Wong et al., 2016), but not yet the CO_2 emissions.

Here we present the quantification of city CO_2 emissions using open-path measurements made with a dual frequency comb spectrometer. While dual-comb spectroscopy is a relatively new technique it has a unique set of attributes that make it attractive for open path measurements (Rieker et al., 2014; Coddington et al., 2016; Waxman et al., 2017; Coburn et al., 2018). Dual-comb spectroscopy (DCS) is a high-resolution, broadband technique spanning hundreds of wavenumbers, but with a resolution that exceeds even high-end FTIRs leading to a negligible instrument lineshape. This allows for simultaneous measurements of multiple species and path-integrated temperature without the need for instrument calibration. Additionally, the eye-safe, high-brightness, single transverse-mode output of a frequency comb allows for beam paths exceeding 10 km while the speed and parallelism of the measurement suppress any spectral distortion from the inevitable turbulence-induced power fluctuations over such a path. Agreement in retrieved concentrations of CO_2 and CH_4 between multiple DCS instruments measuring the same 1 km path has been shown to be as low as 0.14% for CO_2 and 0.35% for CH_4 over a 2 week period (Waxman et al., 2017).

Fig~~ure~~ 1 shows the measurement layout for an initial campaign to quantify CO_2 emissions from Boulder, Colorado. Here we take the light from a dual comb spectrometer near the edge of the city and simultaneously measure two paths: a reference path that points west-southwest towards the mountains and an over-city path that crosses the city to the northeast, covering the main traffic arteries of the city with sensitivity to traffic emissions. We acquire time-resolved data at 32-second resolution of CO_2, CH_4, H_2O and isotopologues over 7.5 weeks. The dry mole fraction of CO_2 and CH_4 show a diurnal cycle expected from anthropogenic sources. In addition, there is a distinct difference between the weekday and weekend cycles for CO_2, consistent with traffic patterns. To estimate the total carbon emission from traffic, we filter the data for days when the wind is out of the west and not too strong so that there is a

Atmos. Chem. Phys. Discuss., https://doi.org/10.5194/acp-2018-796
Manuscript under review for journal Atmos. Chem. Phys.
Discussion started: 3 September 2018

Atmospheric Chemistry and Physics Discussions

measurable daytime enhancement in CO_2 between the reference path and over-city path. We then apply a Gaussian plume model to calculate the city emissions based on the expected distributed source (due to traffic) and the path-averaged concentrations. This emission value is scaled to annual city-wide emissions based on city traffic count data. We estimate $(6.9 \pm 1.8) \times 10^5$ metric tons (MT) CO_2/year, compared to the bottom-up City of Boulder inventory estimate of 4.5×10^5 MT CO_2/year. Finally, we discuss improvements to this estimate, which could be realized by more advantageous beam paths that sample a larger spatial and temporal fraction of the full city emissions.

2. Experimental data

2.1 DCS measurements

The dual frequency comb spectroscopy (DCS) system was located on the top floor of the National Institute of Standards and Technology (NIST) building in Boulder, Colorado. This instrument has been described previously (Truong et al., 2016; Waxman et al., 2017). The light from the combs is split to generate two combined dual-comb outputs, one of which is transmitted over the reference path and one of which is transmitted over the city path (see Fig. 1.) Here, we transmit 2-10 mW of light spanning 1.561 to 1.656 μm, which includes absorption lines from CO_2, CH_4, H_2O and HDO. The returning light from each path is detected and digitized to yield the transmitted optical spectrum at a point spacing of 0.0067 cm^{-1} (1.5 picometer) and with effectively perfect (10 ppb) frequency accuracy and narrow instrument lineshape (~4×10^{-6} cm^{-1}). A typical spectrum from the reference path is shown in Fig. ~~ure~~ 2. A fit of this transmitted spectrum yields the path-averaged gas concentrations. The absolute frequency accuracy and high frequency resolution of the dual-comb spectrometers translates to a high precision and accuracy in the retrieved concentrations. Previously, two DCS instruments measuring atmospheric air were compared over a two-week period and retrieved gas concentrations were found to agree to better than 0.6 ppm for CO_2 and 7 ppb for CH_4 (Waxman et al., 2017). Further, DCS spectra are undistorted by turbulence due to the simultaneous acquisition of all spectral channels and the fast sample rate of the instrument (1.6 ms/spectrum, averaged up to 32 seconds) (Rieker et al., 2014).

For the reference path, 2 mW of dual-comb light is launched from a 2-inch home-built off-axis telescope (Cossel et al., 2017; Waxman et al., 2017). The light travels to a retroreflector located on a hilltop 1 km to the southwest of NIST and then is reflected back to a detector that is co-located with the launch telescope for a 1950.17 ± 0.15 m round-trip path. Return powers vary constantly with air turbulance but we collect about 200 μW for a typical 10 dB link loss. For the city path, 10 mW of dual-comb light is launched from a modified 10-inch diameter astronomical telescope to a retroreflector located on a building roof 3.35 km to the northeast for a 6730.66 ± 0.15 m round-trip path. We collect about 100 μW for a typical 20 dB link loss. Round-trip path distances were measured with a laser range finder. Telescope tracking of the retroreflector is implemented to compensate for thermal drifts via a co-aligned 850 nm light emitting diode (LED) and Silicon CCD camera (Cossel et al., 2017; Waxman et al., 2017).

The measured spectra are analyzed as described in (Rieker et al., 2014; Waxman et al., 2017) at 32 second intervals. Briefly, we fit a 7th-order polynomial and HITRAN data to the measured spectrum in 100-GHz sections to remove the underlying structure from the comb themselves (as opposed to the atmospheric absorption). We fit the resulting absorption spectrum twice: once in the region from 185-188 THz (1.595 to 1.620 μm) to obtain the path-averaged temperature from the 1.6 μm CO_2 band, and once over the entire spectrum to obtain $^{12}CO_2$, $^{13}CO_2$, CH_4, H_2O, and HDO concentrations using the retrieved temperature. We then use the retrieved H_2O concentration to correct the wet CO_2 and CH_4 mole fractions to dry mole fractions, hereafter referred to as X_{CO2} and X_{CH4} given in units of ppm and ppb

(micromole of CO_2 per mole of dry air, and nanomole of CH_4 per mole of dry air). The correction equations are $X_{CO2} = CO_2/(1-H_2O)$ and $X_{CH4} = CH_4/(1-H_2O)$.

2.2 Meteorological Measurements

Meteorological data including pressure, wind direction, and wind speed measurements are obtained from meteorological stations located at NCAR-Mesa and NCAR-Foothills (ftp://ftp.eol.ucar.edu/pub/archive/weather), which are approximately the endpoints of our measurement paths (see Fig. ~~ure~~ 1), as well as a 3-D sonic anemometer located at NIST. The path-averaged air temperature was retrieved from the CO_2 spectra as described above.

2.3 Traffic data

We measure a subset of Boulder traffic, so we use the city traffic data to determine the fraction covered by our footprint (see Fig. ~~ure~~ 1). Traffic data from the City of Boulder is freely available at: https://maps.bouldercolorado.gov/traffic-counts/?_ga=2.264109964.1414067815.1500302174-274759643.1492121882. The city provides two types of traffic data that are useful in this work: the Arterial Count Program (ART) and the Turning Movement Count (TMC) data.

ART measures traffic at 18 major intersections in Boulder for five days (one work week, Monday through Friday) every year in one-hour bins to create a diurnal cycle. The traffic counts for 2016 are shown in Fig. ~~ure~~ 3. We use these data to scale our selected measurement time periods to a full day as discussed in section 3.3.4.

TMC measures the number of vehicles at 140 intersections in Boulder for one work day per year during the hours of 7:45-8:45, 12:00-13:00, and 16:45-17:45. One third of each of these sites is measured every year. We have scaled the 2014 and 2015 data to 2016 traffic levels by using total vehicle mile values available from the City of Boulder. We approximate the location of city vehicle emissions by using the TMC locations as our Gaussian plume source locations with the source strengths scaled based on the location's fractional traffic count. (See Section 3.3.2).

3 Results and Discussion

3.1 DCS measurements

All 7.5 weeks of DCS measurements of CO_2, CH_4, H_2O, and HDO are shown in Fig. ~~ure~~ 4. We have insufficient precision to measure time-resolved $^{13}CO_2$ concentrations over the 2-km path. However, there are very clear enhancements in the over-city path relative to the reference path for the trace gases, especially for CO_2. These enhancements are observed primarily at night when the boundary layer is lower. For example, on Oct. 13 the CO_2 enhancement reaches 129 ppm and the CH_4 enhancement reaches 265 ppb. Daytime enhancements occur when the wind speed is very low and intermittent (typically below 5 m/s), which allows emitted gases to build up over the city. When the wind increases to steady moderate speeds, the concentrations drop quickly as the emissions are flushed out of the city.

3.2 Diurnal Cycles

The diurnal cycle of X_{CO2} and X_{CH4} for both the reference path and the over city path are shown in Fig. ~~ure~~ 5 for weekdays (midnight to midnight Monday through Friday) and weekends (midnight to midnight Saturday and Sunday). We choose to include Monday as a weekday and Saturday as a weekend because the influence of emissions from the previous day is expected to be low. The diurnal cycle of the wind direction and the wind speed measured at NCAR Foothills are also shown in the top panel of Fig. ~~ure~~ 5. All diurnal cycles are the median values over the full 7.5 weeks of measurements.

The diurnal cycle of the reference path CO_2 is nearly flat and nearly identical for both weekends and weekdays. It has only a slight maximum between 9 and 10 am, with average values of 410 to 420

ppm. The flatness of these diurnal cycles supports our assumption that this path represents the reference air entering the city, as there is no buildup over the course of the night as the boundary layer drops.

The diurnal cycle of the city path CO_2 shows a different trend with a stronger diurnal variation. Overnight from about 6 pm (18:00) to 9 am, there is an enhancement in the CO_2 relative to the reference path as the CO_2 from the city sources builds up due to the low winds out of the west and a presumed collapsing nighttime boundary layer. During the weekdays, this enhancement increases in the morning consistent with a commuter traffic peak. After the morning, the combination of the presumed rising boundary layer, increased wind speed, and shift in average wind direction out of the west (270°) to the southeast (135 °) result in a drop in the city path CO_2 so that it matches the reference path CO_2. In the early evening, as the wind speed drops and the wind shifts back to out of the west, the buildup reappears and continues overnight as the boundary layer presumably drops. In general the CO_2 mixing ratios tend to be higher on the weekdays, sometimes exceeding 500 ppm, while weekend mixing ratios are entirely below 490 ppm. This difference is reflected in the median values as well, which reach about 440 ppm during the weekdays but only 430 ppm during the weekend.

The diurnal cycle of the reference path CH_4 is relatively flat for both weekends and weekdays at just over 1.9 ppm, with a slight peak between 9 and 10 am. The diurnal cycle of the city path CH_4 shows an enhancement, relative to the reference path, between midnight and about 9 am. We attribute this enhancement to sources of CH_4 within the city combined again with low nighttime winds and collapsing boundary layer. These sources may be leaking natural gas infrastructure such as observed in Boston (Phillips et al., 2013; McKain et al., 2015; Hendrick et al., 2016), Washington, D.C. (Jackson et al., 2014), and Indianapolis (Lamb et al., 2016). Unlike for CO_2, the CH_4 diurnal cycle appears unrelated to traffic (nor would we expect it to be for clean-burning vehicles) as it does not increase during peak traffic times.

3.3 Estimate for CO_2 emissions due to traffic

3.3.1 Measurement day selections

To select test case days to estimate the city emissions, we filter the X_{CO2} time series for time periods with daytime enhancement and a moderate wind strength predominantly out of the west (270 °). Given the prevailing daytime winds are from the southeast (135°) and often strong, this limits the test case days significantly. However, as is clear from Fig. ~~ure~~ 1, for these wind conditions, the city path samples a significant fraction of the traffic emissions and the reference path samples no traffic emissions. We consider only daytime enhancements because the nighttime boundary layer behavior is significantly more complicated than a well-mixed daytime stable boundary layer. We find two days that meet these criteria: Saturday 22 October 2016 from 11:00 to 16:00. and Tuesday 25 October 2016 from 10:00 to 16:00. Both days have moderate wind speeds (on average, 5 m/s) as measured at both meteorological sites. There are additional days with daytime enhancement in X_{CO2}, but the wind direction is variable. Additionally, there are many days with no daytime enhancement in X_{CO2} because the high wind speeds (6 m/s or higher) prevented buildup of CO_2. We use Oct. 22 as a proxy for all weekend days and Oct. 25 as a proxy for all weekdays. The X_{CO2} and X_{CH4} mixing ratios as well as wind speed and wind direction for these two case study days are shown in Fig. ~~ure~~ 6.

The variability in the reference CO_2 on both days is a real effect. (In processing, any data is removed if the signal power is low, which is indicative of poor telescope alignment or strong weather-related attenuation over the beam path, so the variability is not due to variable signal strength). We observe a weak correlation of the variability with the NCAR Mesa wind speed – approximately 5 minutes prior to most drops in CO_2 there is a spike in the wind speed suggesting that a gust of very clean air has

Atmos. Chem. Phys. Discuss., https://doi.org/10.5194/acp-2018-796
Manuscript under review for journal Atmos. Chem. Phys.
Discussion started: 3 September 2018

Atmospheric Chemistry and Physics Discussions

crossed the measurement path. We see no correlations with other meteorological variables (e.g. temperature, wind direction, pressure).

To convert from the measured enhancement to an emissions rate, we require a model that connects the source strength to the plume concentration. Here, as described below, for this initial demonstration we use a Gaussian plume model although future efforts could employ a more sophisticated model.

3.3.2 Gaussian plume calculations

The standard Gaussian plume model that includes total reflection at the Earth's surface is (Seinfeld and Pandis, 2006):

$$c(x,y,z,t)=\frac{q}{2\pi\sigma_y\sigma_z u}\exp\left(\frac{-(y-y_0)^2}{2\sigma_y^2}\right)\left[\exp\left(\frac{-(z-H)^2}{2\sigma_z^2}\right)+\exp\left(\frac{-(z+H)^2}{2\sigma_z^2}\right)\right] \quad (1)$$

where (x,y,z) is the location in space for which the plume concentration is being calculated, (x_0,y_0,H) is the emissions location, $c(x,y,z,t)$ is the concentration at location (x,y,z) and time t, q is the emissions strength (usually in kg/s), σ_y and σ_z are the plume variances in the y and z direction as a function of travel distance and Pasquill stability class (Seinfeld and Pandis, 2006), and u is the wind speed in m/s. The wind is assumed to be in the x-direction. The plume variances are calculated as:

$$\sigma_y=\exp\left[I_y+J_y(\ln\Delta x)+K_y(\ln\Delta x)^2\right] \quad (2)$$

and

$$\sigma_z=\exp\left[I_z+J_z(\ln\Delta x)+K_z(\ln\Delta x)^2\right] \quad (3)$$

where I_y, J_y, K_y, I_z, J_z, and K_z are from a look-up table based on the Pasquill stability class, which depends on the wind speed and solar insolation (Seinfeld and Pandis, 2006) and Δx is the x-distance relative to the plume origin.

We modify this equation in several ways: 1) Since we measure the column-integrated concentration over a finite beam path at an angle to the wind direction, we integrate the plume concentration along this beam path and then normalize to the length of the beam path. 2) We sum over the emissions locations in the city that contribute emissions to our measurements. Thus our overall measurement equation is:

$$(c-c_0)=\frac{Q}{L}\sum_{(x_j,y_j)}\int_0^L\frac{f_j}{2\pi\sigma_y\sigma_z u}\exp\left(\frac{-(s\sin\theta-y_j)^2}{2\sigma_y^2}\right)\left[\exp\left(\frac{-(15-1)^2}{2\sigma_z^2}\right)+\exp\left(\frac{-(15+1)^2}{2\sigma_z^2}\right)\right]ds \quad (4)$$

where $(c-c_0)$ is our path-integrated concentration enhancement measurement along our path s (in MT/m^3 and MT is metric tons; 1 MT = 1000 kg), Q is the total city emissions in MT/year, L is our path length in m, (x_j,y_j) are the source emissions locations, f_j is the fraction of traffic at source location (x_j,y_j) relative to traffic over all locations in the city from the TMC database, u is the wind speed in m/s, θ is the angle of the beam path with respect to the wind direction, and σ_y and σ_z are the plume dispersions in m in the y and z directions, which depend on the sources distance from the beam path. In writing (4), we assume the wind is in the $+\hat{x}$ direction (which assumption is relaxed below). We assume that all plume emissions locations are emitted from vehicle tailpipes at 1 m above the ground, and the beam path runs 15 m above ground so all measurement heights are at 15 m above ground.

Grid rotation for variable wind directions

To calculate (4), we grid the emissions locations using UTM (Universal Transverse Mercator) coordinates obtained from Google Earth, where we then define north as $+\hat{y}$ and east as $+\hat{x}$. We translate the coordinate system such that the DCS path begins at the origin (0,0) and travels a distance L at angle θ with respect to the x-axis. Eq. (4) is then valid provided the wind is directly in the $+\hat{x}$ direction. More generally, the wind is at a time varying small angle $\phi(t)$ with respect to $+\hat{x}$. Therefore, we apply a rotation about the origin (Prussin et al., 2015):

$$\begin{bmatrix} \cos\phi & \sin\phi \\ -\sin\phi & \cos\phi \end{bmatrix} \begin{bmatrix} x \\ y \end{bmatrix} = \begin{bmatrix} x' \\ y' \end{bmatrix}$$

to generate new traffic coordinates (x_j', y_j') and a new parameterized DCS beam path of $(s\cos(\theta'), s\sin(\theta'))$ where s goes from 0 to L and $\theta' = \theta - \phi(t)$. In this new coordinate system, the wind is along the $+\hat{x}'$ direction and Eq. (4) holds with the substitutions $\theta \to \theta'$ and $y_j \to y'_j$, and where the σ_y and σ_z are calculated based on the distance $\Delta x = \left| x'_j - s_j \cos\theta' \right|$ where $s_j \sin\theta' = y_j$.

Time dependent estimate of $Q(t)$

The rotated Eq. *(4)* can be solved for Q in terms of the measured or estimated values of $c(t) - c_0(t), u(t), \Delta\phi(t), \sigma_y(t), \sigma_z(t), \theta, L, f_i$, where the first five quantities are time dependent. The resulting, time-dependent $Q(t)$ for each test case day is shown in the bottom panels of Fig. 6 and has a mean value and standard deviation of $(5.1 \pm 2.8)\times 10^4$ MT CO_2/year for October 22 and $(6.4 \pm 1.8)\times 10^5$ for October 25. A large part of the variability is driven changes in $c(t) - c_0(t)$ and in $\phi(t)$ (which results in greater or fewer number of plumes from the given traffic locations intercepting the measurement path).

3.3.4 Scaling to annual emissions

The Gaussian plume results are scaled to daily emissions using the hourly traffic data in Fig. ~~ure~~ 3. The traffic data in Fig. ~~ure~~ 3 comes from weekday measurements, but due to the lack of available weekend data we assume that the distribution is the same for weekends. Based on these data, 33% of the total traffic counts on Oct. 22 occur during the 5-hour measurement period and 39% of the total traffic counts on Oct. 25 occur during the 6-hour measurement period. Then we scale to annual emissions by assuming that the emissions on Oct. 22 are representative of all 104 weekend days and the emissions on Oct. 25 are representative of all 261 week days. Scaling the mean values of $Q(t)$ in this way, we estimate an annual emission rate of $(6.9 \pm 1.8)\times 10^5$ MT CO_2/year. The uncertainty is simply the scaled variability in the measured $Q(t)$ and does not include additional uncertainty from scaling to annual emissions or the use of TMC data as a proxy for emissions locations.

3.3.5 Corrections for non-traffic sources of CO_2

We first consider the two power generation facilities on the Department of Commerce campus and collocated with NIST: the Central Utilities Plant (CUP), and the NOAA boilers. To calculate their average CO_2 emissions, we used available fuel consumption data (October 2016 monthly average for the CUP and mid-November to mid-December 2016 average for the NOAA boilers; October data was unavailable) and the EPA emissions factor (EPA, 1995). We then modeled their plume emissions using WindTrax (Flesch et al., 1995, 2004) with wind speed and direction data from the NCAR-Mesa site. We

find that due to the moderate wind speeds (>5 m/s) during our case study days and the height mismatch between the emission stacks and our measurement path over the DOC campus, there should be negligible enhancement. Therefore, we apply no correction for these power plant emissions.

It is also possible that emissions from the University of Colorado power plant could intersect our beam path. The EPA Greenhouse Gas Reporting Program (GHGRP, https://www.epa.gov/ghgreporting) lists the 2016 emission from the power plant as 3.0×10^4 MT CO_2, which is approximately 5% of our calculated emissions value and thus not a significant bias. If we account for the CO_2 from this power plant then our annual vehicle emissions estimate is reduced slightly to $(6.6 \pm 1.8) \times 10^5$ MT/year.

A large power plant lies just outside the city limits to the east of Boulder (the Valmont power station); however, given its location and the dominant westerly wind, emissions from this source should not reach our beam path.

Of course, other small power generation facilities exist within the city that do not report to the GHGRP but may still produce emissions that intersect our beam path. Certainly, there are diffuse emissions from residential and commercial furnaces and water heaters. We likely also measure contributions from plant and soil respiration as these measurements were made in the late fall when photosynthesis was likely minimal but respiration was likely ongoing because the temperatures were above freezing. Respiration was found to be a significant source of CO_2 emissions in Indianapolis (Gurney et al., 2017). As with the emissions from furnaces or smaller generation facilities, we have not attempted to quantify or correct for this effect, which could inflate our estimate.

3.3.6 Uncertainty discussion

Uncertainty in mean values $\langle Q(t) \rangle$ for the test case days

Seven measured parameters factor in to the emissions calculation of $Q(t)$ for the two days. These are given in Table I along with the instrumental measurement precision and the observed variability. In terms of instrument uncertainty, the precision of the retrieved CO_2 is 0.9 ppm for the reference path at our 30-second time resolution (Waxman et al., 2017) and 0.5 ppm for the over-city path. The precision is better over the longer path because the absorption lines are stronger. Note that solar insolation is used solely in the determination of the Pasquill stability class (Seinfeld and Pandis, 2006). The stability class is relatively insensitive to the variations in solar insolation observed on the two test case days. As can be seen in the table, the uncertainty is dominated by the natural variability in parameters like wind speed, wind direction, and CO_2 concentration rather than the instrument precision. The observed variability over the 5-6 hour period is typically at least a factor of 2 larger than the instrument precision. The variability in these parameters leads to the observed variability in $Q(t)$. We use the mean of $Q(t)$ as our emissions value and the standard deviation as its uncertainty. In using this standard deviation as a measure of the uncertainty, we attempt to capture the uncertainty associated with the discrepancies between, for example, the weather-station measurements of wind direction and speed relative to the true wind speed and direction across our distributed path. For example, slight shifts in wind direction will cause plumes from different traffic locations to intersect or not intersect the beam path. This variability appears in the calculated $Q(t)$ as the nominal measured wind direction varies. Future systems with redundant, distributed DCS beam paths would provide a superior estimate of all these uncertainties.

Uncertainty in the scaling to city-wide annual emissions

Values supplied by the city of Boulder – traffic count data and emissions inventory numbers – do not have an associated uncertainty value. However, even if there was negligible uncertainty on the

measurements, there is inherent statistical uncertainty in the strong extrapolation from our 5-6 hour period to a full day and then to the entire year. Moreover, the traffic data used to scale the emissions up from 6 hours to 24 hours was collected solely on week days, which might lead to a slight overestimate in the weekend data because a larger fraction of the weekend emissions occur between 11 am and 4 pm than weekday emissions. Obviously, the extrapolation also misses seasonality in the emissions. Further, implicitly built in to Equation 4 is a spatial scaling that uses discrete points from a subsection of the city (those emissions locations whose beam paths cross our measurement path). The systematic uncertainty in this spatial and temporal scaling from our measurements to annual city emissions is unknown but possibly substantial. Without additional information, it is not possible to add additional uncertainty to the current 26% uncertainty, which is based solely on the measured variability in $Q(t)$.

Assumptions required for the Gaussian plume model

There are a number of assumptions inherent to the Gaussian plume model. For example, it does not include the effects of buildings, trees, or other objects that could break up the plume between the emissions location and the beam path. Further, even within the Gaussian plume model, we make a number of assumptions. We assume that all CO_2 emissions come from the discrete locations shown in Fig~~ure~~ 1, while in reality the emissions are likely substantially more diffuse. The assumption of discrete emissions simplifies modeling and is feasible due to the city traffic data, but may result in a bias due to the coarse distribution of traffic measurements. We approximate that all emissions are released at 1 m above ground (vehicle tailpipes) and are measured at 15 m above ground. In reality, the beam height differs over the path since Boulder is not perfectly flat. Finally, we use standard I_y, J_y, K_y, I_z, J_z, and K_z values which were derived for rural areas (Turner, 1970) which may be different than urban or suburban areas. However, the greatest differences between rural and urban conditions are expected to be at night (Turner, 1970).

4 Comparison with city estimates

The City vehicle emissions estimate comes from total vehicle miles traveled based on data from the Transportation department, miles per gallon inputs from the EPA state inventory tool, and vehicle type distribution from the Colorado Department of Public Health and the Environment (Kimberlee Rankin, City of Boulder, personal communication).The City of Boulder estimates that the total vehicle emissions were 4.47×10^5 metric tons (MT) of CO_2 equivalent (CO_2e) in 2015, the most recent year of the city greenhouse gas inventory. When scaled up to 2016 levels based on total vehicle miles traveled (8.98×10^8 miles in 2015 and 9.09×10^8 miles in 2016), this is 4.52×10^5 MT CO2e in 2016. We assume that all traffic emissions are CO_2 rather than a mix of CO_2 and CH_4. There is no uncertainty provided by the city on this value.

In comparison, we estimate $(6.9 \pm 1.8) \times 10^5$ MT CO_2/year, which is 155% of the city estimate. While the discrepancy is moderately large it is reasonable agreement for a top down measurement and bottom up inventory comparison, especially given that there are possibly additional CO_2 sources contributing to our measured values that we are currently unable to quantify. Other studies have also found that emissions measurements were higher than the reported inventory values. Brioude et al., (2013) found top-down aircraft estimates of Los Angeles county and the South Coast Air Basin (SoCAB) CO_2 were 1.45 times larger than the Vulcan 2005 inventory (Gurney et al., 2009). An earlier aircraft campaign over Sacramento, CA found an average CO_2 emission, with 100% uncertainty, that was 15-20% higher than the Vulcan estimate (Turnbull et al., 2011). Lauvaux et al. (2016) compared Indianapolis city CO_2 emissions measured by a network of CRDS instruments to the HESTIA inventory (Gurney et al., 2012) during INFLUX (Davis et al., 2017). They found that despite the building-scale resolution in the HESTIA inventory, it still under-estimated the annual CO_2 flux by 20%. An updated version of HESTIA

predicted very similar emissions estimates for on-road, residential, and commercial sectors, so the discrepancy was attributed to missing sources of CO_2, including animal (primarily human and companion animal) respiration, biofuel combustion, and biosphere respiration (Gurney et al., 2017).

4.1 Improvements in future measurements

Future improvements should include additional and different beam paths, selected based on prevailing wind directions. (Our initial assumption that the mountain path would generally act as a reference path was incorrect since the prevailing daytime winds are not out of the west but rather the southeast.) An east-west running beam north of the city and one south of the city would allow us to utilize a larger fraction of the data as the predominant midday wind direction during the fall is out of the north to north-east (see Fig. ~~ure~~ 5). Even longer beam paths would also interrogate a larger fraction of the city and measure a correspondingly larger fraction of the vehicle emissions. Vertically-resolved data from e.g. a series of stacked retroreflectors would better test the assumption of vertically-dispersing Gaussian plumes.

Additionally, more extensive modeling to cover variable wind directions and speeds would allow the incorporation of a much larger fraction of the data than the two days selected here. An inversion-based model similar to (Lauvaux et al., 2013) could potentially be applied to a small city like Boulder; however this would depend heavily on the quality of the bottom-up emissions inventory used to generate the priors.

5 Conclusions

We demonstrate the use of an open-path dual frequency comb spectroscopy system for quantifying city emissions of carbon dioxide. We send light over two paths: a reference path that samples the concentration of gases entering the city from the west, and an over-city path that measures the concentrations of gases after the air mass has crossed approximately two-thirds of the city including two major commuter arteries. The measured diurnal cycle shows a significant commuter peak in the carbon dioxide signal during weekdays in the over-city path compared to the reference path. We select two case study days with appropriate wind conditions and apply Gaussian plume modeling to estimate the total vehicular carbon emission. We then scale these results up to annual city-wide emissions using traffic data from the City of Boulder. We find overall traffic related carbon emissions that are approximately 1.55 times greater than the city's bottom-up traffic emissions inventory. This is reasonably good agreement given the limited number of measurement days that were suitable for the modeling and assumptions in the use of a Gaussian plume model. Further improvements to this method should include improved design of reference and over-city paths, enabling this method to be used for multiple wind directions.

Acknowledgements: We thank Kimberlee Rankin, Randall Rutsch, Bill Cowern, and Chris Hagelin from the City of Boulder for city inventory and traffic information and ~~xx~~ Dave Plusquellic and ~~xx~~ Caroline Alden for assistance with the manuscript. This work was funded by Defense Advanced Research Program Agency DSO SCOUT program, and James Whetstone and the NIST special program office. Eleanor M. Waxman and Kevin C. Cossel are partially supported by National Research Council postdoctoral fellowships.

5. References

Allen, D. T.: Methane emissions from natural gas production and use: reconciling bottom-up and top-down measurements, Curr. Opin. Chem. Eng., 5, 78–83, doi:10.1016/j.coche.2014.05.004, 2014.

456 Bergeron, O. and Strachan, I. B.: CO_2 sources and sinks in urban and suburban areas of a
457 northern mid-latitude city, Atmos. Environ., 45(8), 1564–1573,
458 doi:10.1016/j.atmosenv.2010.12.043, 2011.

459 Bréon, F. M., Broquet, G., Puygrenier, V., Chevallier, F., Xueref-Remy, I., Ramonet, M.,
460 Dieudonné, E., Lopez, M., Schmidt, M., Perrussel, O. and Ciais, P.: An attempt at estimating
461 Paris area CO_2 emissions from atmospheric concentration measurements, Atmos Chem Phys,
462 15(4), 1707–1724, doi:10.5194/acp-15-1707-2015, 2015.

463 Brioude, J., Angevine, W. M., Ahmadov, R., Kim, S.-W., Evan, S., McKeen, S. A., Hsie, E.-Y.,
464 Frost, G. J., Neuman, J. A., Pollack, I. B., Peischl, J., Ryerson, T. B., Holloway, J., Brown, S. S.,
465 Nowak, J. B., Roberts, J. M., Wofsy, S. C., Santoni, G. W., Oda, T. and Trainer, M.: Top-down
466 estimate of surface flux in the Los Angeles Basin using a mesoscale inverse modeling technique:
467 assessing anthropogenic emissions of CO, NO_x and CO_2 and their impacts, Atmos Chem Phys,
468 13(7), 3661–3677, doi:10.5194/acp-13-3661-2013, 2013.

469 Ciais, P., Rayner, P., Chevallier, F., Bousquet, P., Logan, M., Peylin, P. and Ramonet, M.:
470 Atmospheric inversions for estimating CO_2 fluxes: methods and perspectives, Clim. Change,
471 103(1–2), 69–92, doi:10.1007/s10584-010-9909-3, 2010.

472 Coburn, S., Alden, C. B., Wright, R., Cossel, K., Baumann, E., Truong, G.-W., Giorgetta, F.,
473 Sweeney, C., Newbury, N. R., Prasad, K., Coddington, I. and Rieker, G. B.: Regional trace-gas
474 source attribution using a field-deployed dual frequency comb spectrometer, Optica, 5(4), 320–
475 327, doi:10.1364/OPTICA.5.000320, 2018.

476 Coddington, I., Newbury, N. and Swann, W.: Dual-comb spectroscopy, Optica, 3(4), 414,
477 doi:10.1364/OPTICA.3.000414, 2016.

478 Cossel, K. C., Waxman, E. M., Giorgetta, F. R., Cermak, M., Coddington, I. R., Hesselius, D.,
479 Ruben, S., Swann, W. C., Truong, G.-W., Rieker, G. B. and Newbury, N. R.: Open-path dual-
480 comb spectroscopy to an airborne retroreflector, Optica, 4(7), 724–728,
481 doi:10.1364/OPTICA.4.000724, 2017.

482 Coutts, A. M., Beringer, J. and Tapper, N. J.: Characteristics influencing the variability of urban
483 CO_2 fluxes in Melbourne, Australia, Atmos. Environ., 41(1), 51–62,
484 doi:10.1016/j.atmosenv.2006.08.030, 2007.

485 Davis, K. J., Deng, A., Lauvaux, T., Miles, N. L., Richardson, S. J., Sarmiento, D. P., Gurney, K.
486 R., Hardesty, R. M., Bonin, T. A., Brewer, W. A., Lamb, B. K., Shepson, P. B., Harvey, R. M.,
487 Cambaliza, M. O., Sweeney, C., Turnbull, J. C., Whetstone, J. and Karion, A.: The Indianapolis
488 Flux Experiment (INFLUX): A test-bed for developing urban greenhouse gas emission
489 measurements, Elem Sci Anth, 5(0), 21, doi:10.1525/elementa.188, 2017.

490 Dobler, J. T., Zaccheo, T. S., Pernini, T. G., Blume, N., Broquet, G., Vogel, F., Ramonet, M.,
491 Braun, M., Staufer, J., Ciais, P. and Botos, C.: Demonstration of spatial greenhouse gas mapping
492 using laser absorption spectrometers on local scales, J. Appl. Remote Sens., 11(1), 014002,
493 doi:10.1117/1.JRS.11.014002, 2017.

494 EPA: AP 42, Fifth Edition Compilation of Air Pollutant Emissions Factors, Volume 1:
495 Stationary Point and Area Sources, [online] Available from: https://www.epa.gov/air-emissions-
496 factors-and-quantification/ap-42-compilation-air-emission-factors#5thed, 1995.

497 Flesch, T. K., Wilson, J. D. and Yee, E.: Backward-Time Lagrangian Stochastic Dispersion
498 Models and Their Application to Estimate Gaseous Emissions, J. Appl. Meteorol., 34(6), 1320–
499 1332, doi:10.1175/1520-0450(1995)034<1320:BTLSDM>2.0.CO;2, 1995.

500 Flesch, T. K., Wilson, J. D., Harper, L. A., Crenna, B. P. and Sharpe, R. R.: Deducing Ground-
501 to-Air Emissions from Observed Trace Gas Concentrations: A Field Trial, J. Appl. Meteorol.,
502 43(3), 487–502, doi:10.1175/1520-0450(2004)043<0487:DGEFOT>2.0.CO;2, 2004.

503 Gurney, K. R., Mendoza, D. L., Zhou, Y., Fischer, M. L., Miller, C. C., Geethakumar, S. and Du
504 Can, S. D. L. R.: High Resolution Fossil Fuel Combustion CO_2 Emission Fluxes for the United
505 States, Environ. Sci. Technol., 43(14), 5535–5541, doi:10.1021/es900806c, 2009.

506 Gurney, K. R., Razlivanov, I., Song, Y., Zhou, Y., Benes, B. and Abdul-Massih, M.:
507 Quantification of Fossil Fuel CO_2 Emissions on the Building/Street Scale for a Large U.S. City,
508 Environ. Sci. Technol., 46(21), 12194–12202, doi:10.1021/es3011282, 2012.

509 Gurney, K. R., Liang, J., Patarasuk, R., O'Keeffe, D., Huang, J., Hutchins, M., Lauvaux, T.,
510 Turnbull, J. C. and Shepson, P. B.: Reconciling the differences between a bottom-up and inverse-
511 estimated $FFCO_2$ emissions estimate in a large US urban area, Elem Sci Anth, 5(0),
512 doi:10.1525/elementa.137, 2017.

513 Heimburger, A. M. F., Harvey, R. M., Shepson, P. B., Stirm, B. H., Gore, C., Turnbull, J.,
514 Cambaliza, M. O. L., Salmon, O. E., Kerlo, A.-E. M., Lavoie, T. N., Davis, K. J., Lauvaux, T.,
515 Karion, A., Sweeney, C., Brewer, W. A., Hardesty, R. M. and Gurney, K. R.: Assessing the
516 optimized precision of the aircraft mass balance method for measurement of urban greenhouse
517 gas emission rates through averaging, Elem Sci Anth, 5(0), doi:10.1525/elementa.134, 2017.

518 Hendrick, M. F., Ackley, R., Sanaie-Movahed, B., Tang, X. and Phillips, N. G.: Fugitive
519 methane emissions from leak-prone natural gas distribution infrastructure in urban environments,
520 Environ. Pollut., 213, 710–716, doi:10.1016/j.envpol.2016.01.094, 2016.

521 Jackson, R. B., Down, A., Phillips, N. G., Ackley, R. C., Cook, C. W., Plata, D. L. and Zhao, K.:
522 Natural Gas Pipeline Leaks Across Washington, DC, Environ. Sci. Technol., 48(3), 2051–2058,
523 doi:10.1021/es404474x, 2014.

524 Karion, A., Sweeney, C., Pétron, G., Frost, G., Michael Hardesty, R., Kofler, J., Miller, B. R.,
525 Newberger, T., Wolter, S., Banta, R., Brewer, A., Dlugokencky, E., Lang, P., Montzka, S. A.,
526 Schnell, R., Tans, P., Trainer, M., Zamora, R. and Conley, S.: Methane emissions estimate from
527 airborne measurements over a western United States natural gas field, Geophys. Res. Lett.,
528 40(16), 4393–4397, doi:10.1002/grl.50811, 2013.

529 Karion, A., Sweeney, C., Kort, E. A., Shepson, P. B., Brewer, A., Cambaliza, M., Conley, S. A.,
530 Davis, K., Deng, A., Hardesty, M., Herndon, S. C., Lauvaux, T., Lavoie, T., Lyon, D.,
531 Newberger, T., Pétron, G., Rella, C., Smith, M., Wolter, S., Yacovitch, T. I. and Tans, P.:

Aircraft-Based Estimate of Total Methane Emissions from the Barnett Shale Region, Environ. Sci. Technol., 49(13), 8124–8131, doi:10.1021/acs.est.5b00217, 2015.

Lamb, B. K., Cambaliza, M. O. L., Davis, K. J., Edburg, S. L., Ferrara, T. W., Floerchinger, C., Heimburger, A. M. F., Herndon, S., Lauvaux, T., Lavoie, T., Lyon, D. R., Miles, N., Prasad, K. R., Richardson, S., Roscioli, J. R., Salmon, O. E., Shepson, P. B., Stirm, B. H. and Whetstone, J.: Direct and Indirect Measurements and Modeling of Methane Emissions in Indianapolis, Indiana, Environ. Sci. Technol., 50(16), 8910–8917, doi:10.1021/acs.est.6b01198, 2016.

Lauvaux, T., Miles, N. L., Richardson, S. J., Deng, A., Stauffer, D. R., Davis, K. J., Jacobson, G., Rella, C., Calonder, G.-P. and DeCola, P. L.: Urban Emissions of CO_2 from Davos, Switzerland: The First Real-Time Monitoring System Using an Atmospheric Inversion Technique, J. Appl. Meteorol. Climatol., 52(12), 2654–2668, doi:10.1175/JAMC-D-13-038.1, 2013.

Lauvaux, T., Miles, N. L., Deng, A., Richardson, S. J., Cambaliza, M. O., Davis, K. J., Gaudet, B., Gurney, K. R., Huang, J., O'Keefe, D., Song, Y., Karion, A., Oda, T., Patarasuk, R., Razlivanov, I., Sarmiento, D., Shepson, P., Sweeney, C., Turnbull, J. and Wu, K.: High-resolution atmospheric inversion of urban CO_2 emissions during the dormant season of the Indianapolis Flux Experiment (INFLUX), J. Geophys. Res. Atmospheres, 121(10), 2015JD024473, doi:10.1002/2015JD024473, 2016.

Marcotullio, P. J., Sarzynski, A., Albrecht, J., Schulz, N. and Garcia, J.: The geography of global urban greenhouse gas emissions: an exploratory analysis, Clim. Change, 121(4), 621–634, doi:10.1007/s10584-013-0977-z, 2013.

Mays, K. L., Shepson, P. B., Stirm, B. H., Karion, A., Sweeney, C. and Gurney, K. R.: Aircraft-Based Measurements of the Carbon Footprint of Indianapolis, Environ. Sci. Technol., 43(20), 7816–7823, doi:10.1021/es901326b, 2009.

McKain, K., Wofsy, S. C., Nehrkorn, T., Eluszkiewicz, J., Ehleringer, J. R. and Stephens, B. B.: Assessment of ground-based atmospheric observations for verification of greenhouse gas emissions from an urban region, Proc. Natl. Acad. Sci., 109(22), 8423–8428, doi:10.1073/pnas.1116645109, 2012.

McKain, K., Down, A., Raciti, S. M., Budney, J., Hutyra, L. R., Floerchinger, C., Herndon, S. C., Nehrkorn, T., Zahniser, M. S., Jackson, R. B., Phillips, N. and Wofsy, S. C.: Methane emissions from natural gas infrastructure and use in the urban region of Boston, Massachusetts, Proc. Natl. Acad. Sci., 112(7), 1941–1946, doi:10.1073/pnas.1416261112, 2015.

Mueller, K., Yadav, V., Lopez-Coto, I., Karion, A., Gourdji, S., Martin, C. and Whetstone, J.: Siting background towers to characterize incoming air for urban greenhouse gas estimation: a case study in the Washington DC/Baltimore Area, J. Geophys. Res. Atmospheres, 2017JD027364, doi:10.1002/2017JD027364, 2017.

Nemitz, E., Hargreaves, K. J., McDonald, A. G., Dorsey, J. R. and Fowler, D.: Micrometeorological Measurements of the Urban Heat Budget and CO_2 Emissions on a City Scale, Environ. Sci. Technol., 36(14), 3139–3146, doi:10.1021/es010277e, 2002.

571 Phillips, N. G., Ackley, R., Crosson, E. R., Down, A., Hutyra, L. R., Brondfield, M., Karr, J. D.,
572 Zhao, K. and Jackson, R. B.: Mapping urban pipeline leaks: Methane leaks across Boston,
573 Environ. Pollut., 173(Supplement C), 1–4, doi:10.1016/j.envpol.2012.11.003, 2013.

574 Prussin, A. J., Marr, L. C., Schmale, D. G., Stoll, R. and Ross, S. D.: Experimental validation of
575 a long-distance transport model for plant pathogens: Application to Fusarium graminearum,
576 Agric. For. Meteorol., 203, 118–130, doi:10.1016/j.agrformet.2014.12.009, 2015.

577 Rieker, G. B., Giorgetta, F. R., Swann, W. C., Kofler, J., Zolot, A. M., Sinclair, L. C., Baumann,
578 E., Cromer, C., Petron, G., Sweeney, C., Tans, P. P., Coddington, I. and Newbury, N. R.:
579 Frequency-comb-based remote sensing of greenhouse gases over kilometer air paths, Optica,
580 1(5), 290–298, doi:10.1364/OPTICA.1.000290, 2014.

581 Ryerson, T. B., Trainer, M., Holloway, J. S., Parrish, D. D., Huey, L. G., Sueper, D. T., Frost, G.
582 J., Donnelly, S. G., Schauffler, S., Atlas, E. L., Kuster, W. C., Goldan, P. D., Hübler, G.,
583 Meagher, J. F. and Fehsenfeld, F. C.: Observations of Ozone Formation in Power Plant Plumes
584 and Implications for Ozone Control Strategies, Science, 292(5517), 719–723,
585 doi:10.1126/science.1058113, 2001.

586 Seinfeld, J. H. and Pandis, S. N.: Atmospheric Chemistry and Physics: From Air Pollution to
587 Climate Change, Wiley., 2006.

588 Seto, K. C., Bigio, A., Bento, A., Cervero, R. and Christensen, P.: Human Settlements,
589 Infrastructure, and Spatial Planning, in Climate Change 2014: Mitigation of Coimate Change.
590 Contribution of Working Group III to the Fifth Assessment Report of the Intergovernmental
591 Panel on Climate Change, p. 78., 2014.

592 Shusterman, A. A., Teige, V. E., Turner, A. J., Newman, C., Kim, J. and Cohen, R. C.: The
593 BErkeley Atmospheric CO_2 Observation Network: initial evaluation, Atmos Chem Phys, 16(21),
594 13449–13463, doi:10.5194/acp-16-13449-2016, 2016.

595 Staufer, J., Broquet, G., Bréon, F.-M., Puygrenier, V., Chevallier, F., Xueref-Rémy, I.,
596 Dieudonné, E., Lopez, M., Schmidt, M., Ramonet, M., Perrussel, O., Lac, C., Wu, L. and Ciais,
597 P.: The first 1-year-long estimate of the Paris region fossil fuel CO_2 emissions based on
598 atmospheric inversion, Atmos Chem Phys, 16(22), 14703–14726, doi:10.5194/acp-16-14703-
599 2016, 2016.

600 Truong, G.-W., Waxman, E. M., Cossel, K. C., Baumann, E., Klose, A., Giorgetta, F. R., Swann,
601 W. C., Newbury, N. R. and Coddington, I.: Accurate frequency referencing for fieldable dual-
602 comb spectroscopy, Opt. Express, 24(26), 30495–30504, doi:10.1364/OE.24.030495, 2016.

603 Turnbull, J. C., Karion, A., Fischer, M. L., Faloona, I., Guilderson, T., Lehman, S. J., Miller, B.
604 R., Miller, J. B., Montzka, S., Sherwood, T., Saripalli, S., Sweeney, C. and Tans, P. P.:
605 Assessment of fossil fuel carbon dioxide and other anthropogenic trace gas emissions from
606 airborne measurements over Sacramento, California in spring 2009, Atmos Chem Phys, 11(2),
607 705–721, doi:10.5194/acp-11-705-2011, 2011.

608 Turner, D. B.: Workbook of Atmospheric Dispersion Estimates, [online] Available from:
609 https://ia802704.us.archive.org/4/items/workbookofatmosp026353mbp/workbookofatmosp0263
610 53mbp.pdf (Accessed 5 June 2017), 1970.

611 Velasco, E., Pressley, S., Allwine, E., Westberg, H. and Lamb, B.: Measurements of CO_2 fluxes
612 from the Mexico City urban landscape, Atmos. Environ., 39(38), 7433–7446,
613 doi:10.1016/j.atmosenv.2005.08.038, 2005.

614 Velasco, E., Perrusquia, R., Jiménez, E., Hernández, F., Camacho, P., Rodríguez, S., Retama, A.
615 and Molina, L. T.: Sources and sinks of carbon dioxide in a neighborhood of Mexico City,
616 Atmos. Environ., 97(Supplement C), 226–238, doi:10.1016/j.atmosenv.2014.08.018, 2014.

617 Waxman, E. M., Cossel, K. C., Truong, G.-W., Giorgetta, F. R., Swann, W. C., Coburn, S.,
618 Wright, R. J., Rieker, G. B., Coddington, I. and Newbury, N. R.: Intercomparison of open-path
619 trace gas measurements with two dual-frequency-comb spectrometers, Atmos Meas Tech, 10(9),
620 3295–3311, doi:10.5194/amt-10-3295-2017, 2017.

621 White, W. H., Anderson, J. A., Blumenthal, D. L., Husar, R. B., Gillani, N. V., Husar, J. D. and
622 Wilson, W. E.: Formation and transport of secondary air pollutants: ozone and aerosols in the St.
623 Louis urban plume, Science, 194(4261), 187–189, doi:10.1126/science.959846, 1976.

624 Wong, C. K., Pongetti, T. J., Oda, T., Rao, P., Gurney, K. R., Newman, S., Duren, R. M., Miller,
625 C. E., Yung, Y. L. and Sander, S. P.: Monthly trends of methane emissions in Los Angeles from
626 2011 to 2015 inferred by CLARS-FTS observations, Atmos Chem Phys, 16(20), 13121–13130,
627 doi:10.5194/acp-16-13121-2016, 2016.

628 Wunch, D., Wennberg, P. O., Toon, G. C., Keppel-Aleks, G. and Yavin, Y. G.: Emissions of
629 greenhouse gases from a North American megacity, Geophys. Res. Lett., 36(15), L15810,
630 doi:10.1029/2009GL039825, 2009.

631 Ye, X., Lauvaux, T., Kort, E. A., Oda, T., Feng, S., Lin, J. C., Yang, E. and Wu, D.:
632 Constraining fossil fuel CO_2 emissions from urban area using OCO-2 observations of total
633 column CO_2, Atmospheric Chem. Phys. Discuss., 1–30, doi:https://doi.org/10.5194/acp-2017-
634 1022, 2017.

635 Zavala-Araiza, D., Lyon, D. R., Alvarez, R. A., Davis, K. J., Harriss, R., Herndon, S. C., Karion,
636 A., Kort, E. A., Lamb, B. K., Lan, X., Marchese, A. J., Pacala, S. W., Robinson, A. L., Shepson,
637 P. B., Sweeney, C., Talbot, R., Townsend-Small, A., Yacovitch, T. I., Zimmerle, D. J. and
638 Hamburg, S. P.: Reconciling divergent estimates of oil and gas methane emissions, Proc. Natl.
639 Acad. Sci., 112(51), 15597–15602, doi:10.1073/pnas.1522126112, 2015.

640
641

Atmos. Chem. Phys. Discuss., https://doi.org/10.5194/acp-2018-796
Manuscript under review for journal Atmos. Chem. Phys.
Discussion started: 3 September 2018

Atmospheric Chemistry and Physics Discussions

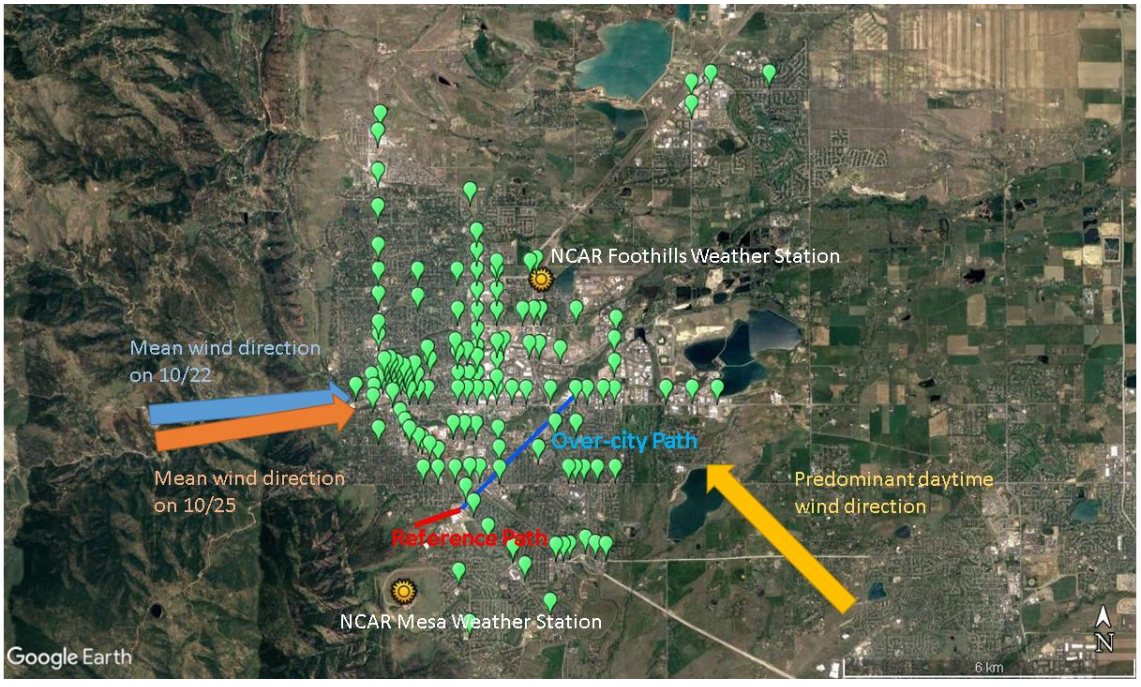

Figure 1: Measurement layout. The two measurement paths are shown by red (reference) and blue (over-city) lines. The two weather stations that provided wind speed and direction data are given by the sun symbols. The green markers are TMC locations and the Gaussian plume source locations. Dominant wind directions for the campaign overall and the test case days are given by colored arrows. Data: Google, USDA, USGS, Digital Globe

Atmos. Chem. Phys. Discuss., https://doi.org/10.5194/acp-2018-796
Manuscript under review for journal Atmos. Chem. Phys.
Discussion started: 3 September 2018

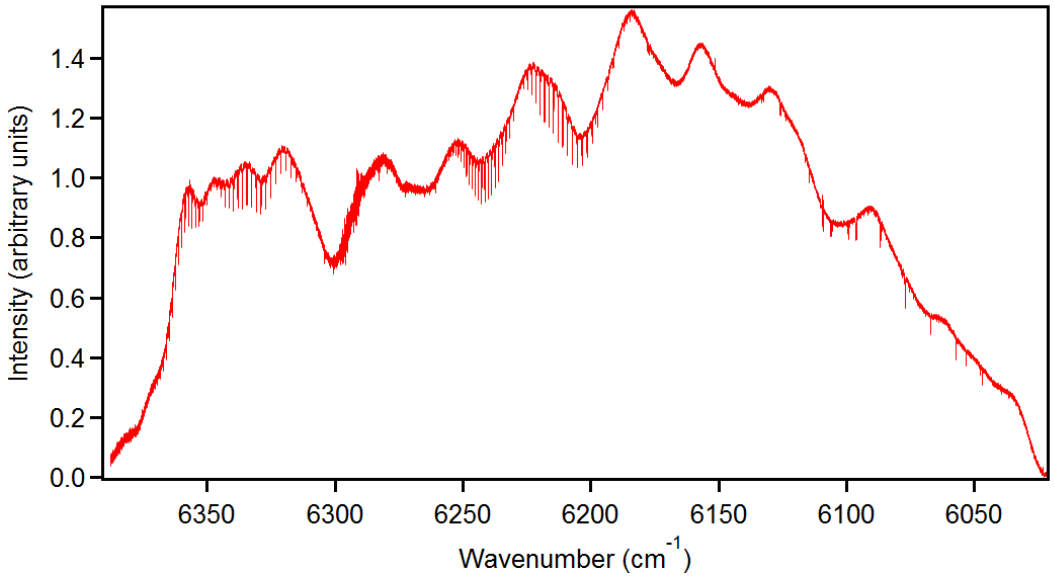

Figure 2: Typical 32-second spectrum measured over the 2-km reference path. CO_2 bands are observed in the 6350 cm^{-1} and 6225 cm^{-1} regions, while CH_4 and H_2O are measured between 6150 and 6050 cm^{-1}. The larger, slowly varying structure is from the comb spectra. The atmospheric absorption appears as the small and narrow dips.

Atmos. Chem. Phys. Discuss., https://doi.org/10.5194/acp-2018-796
Manuscript under review for journal Atmos. Chem. Phys.
Discussion started: 3 September 2018

Atmospheric Chemistry and Physics Discussions

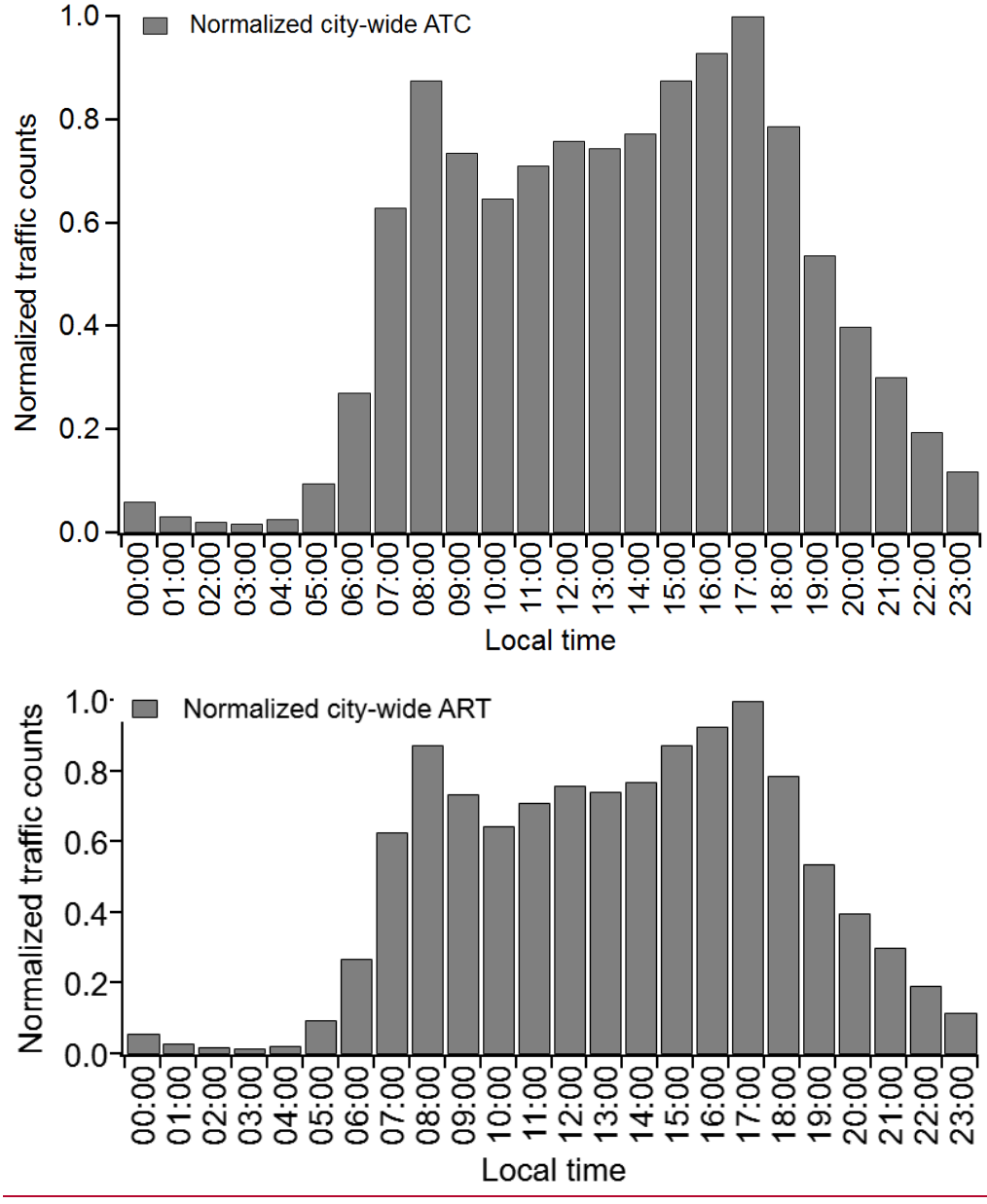

Figure 3: City-wide traffic counts for determining diurnal cycle, normalized to a peak of unity.

Atmos. Chem. Phys. Discuss., https://doi.org/10.5194/acp-2018-796
Manuscript under review for journal Atmos. Chem. Phys.
Discussion started: 3 September 2018

Atmospheric Chemistry and Physics Discussions

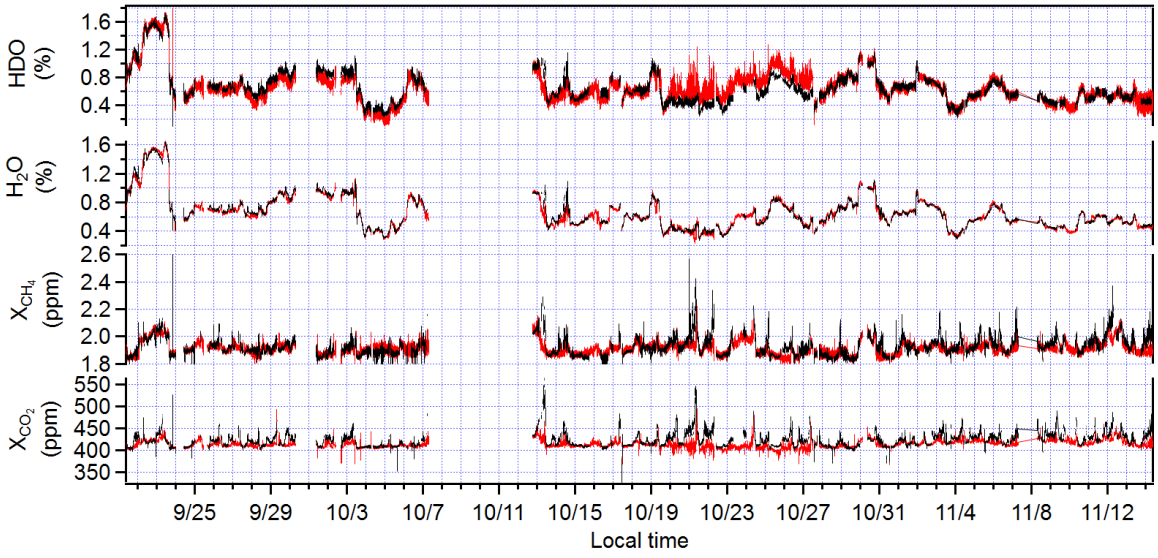

Figure 4: 7.5 weeks of dual-comb spectroscopy data for the reference path (red) and the over-city path (black). Enhancements in the over-city path relative to the reference path are observed in CO_2 and CH_4 but not in H_2O or HDO. (Note: the HDO concentration includes the HITRAN isotopic scaling.)

Atmos. Chem. Phys. Discuss., https://doi.org/10.5194/acp-2018-796
Manuscript under review for journal Atmos. Chem. Phys.
Discussion started: 3 September 2018

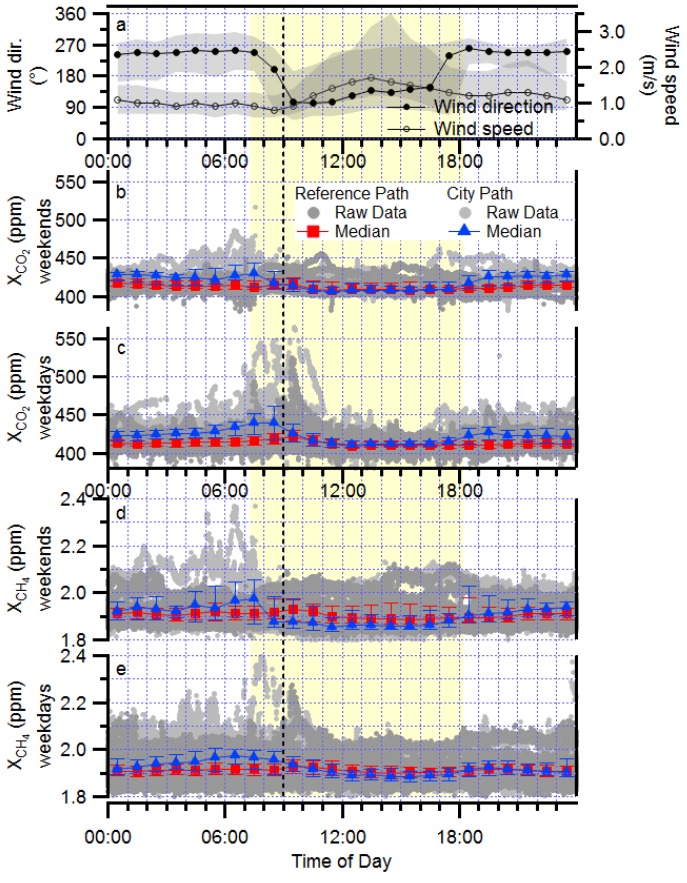

671
672

Atmos. Chem. Phys. Discuss., https://doi.org/10.5194/acp-2018-796
Manuscript under review for journal Atmos. Chem. Phys.
Discussion started: 3 September 2018

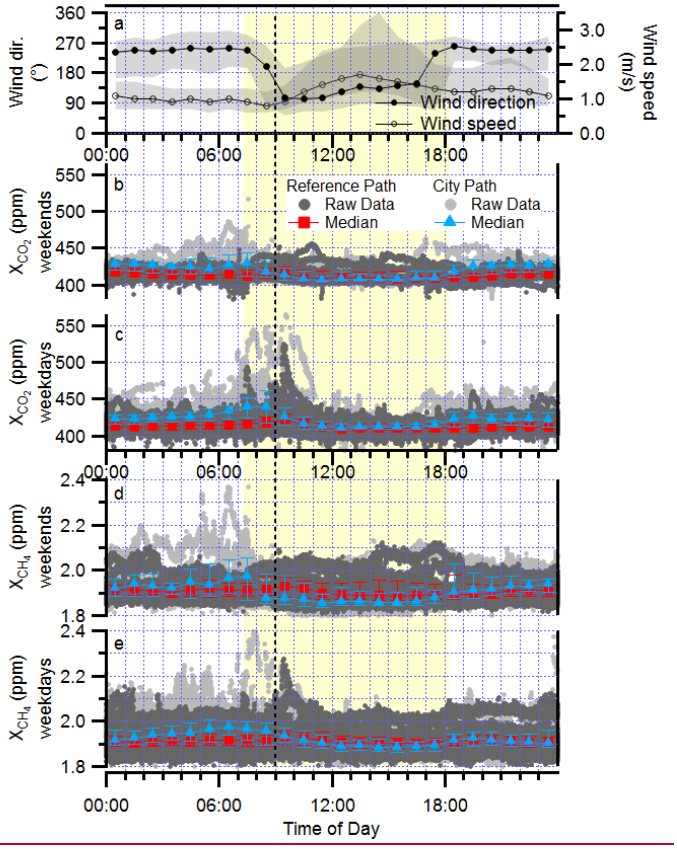

Figure 5: Diurnal cycle analysis. Data is the median of the full 7.5 weeks. (a) The mean wind direction as measured from its origin (black trace, left axis) and wind speed (gray trace, right axis) both from the NCAR Foothills measurement station, shaded regions reflect the 25th to 75th quartiles; (b) the weekend and (c) weekday X_{CO2} over the city path (light grey dots) and reference path (dark gray dots) over all days as well as median values for the over-city path (blue triangles) and reference path (red squares). (d) and (e) Same data for X_{CH4}. The vertical dashed black line marks 9:00 local time and the yellow shaded region highlights the region from sunrise to sunset on Oct. 22, 2016.

Atmos. Chem. Phys. Discuss., https://doi.org/10.5194/acp-2018-796
Manuscript under review for journal Atmos. Chem. Phys.
Discussion started: 3 September 2018

Atmospheric Chemistry and Physics Discussions

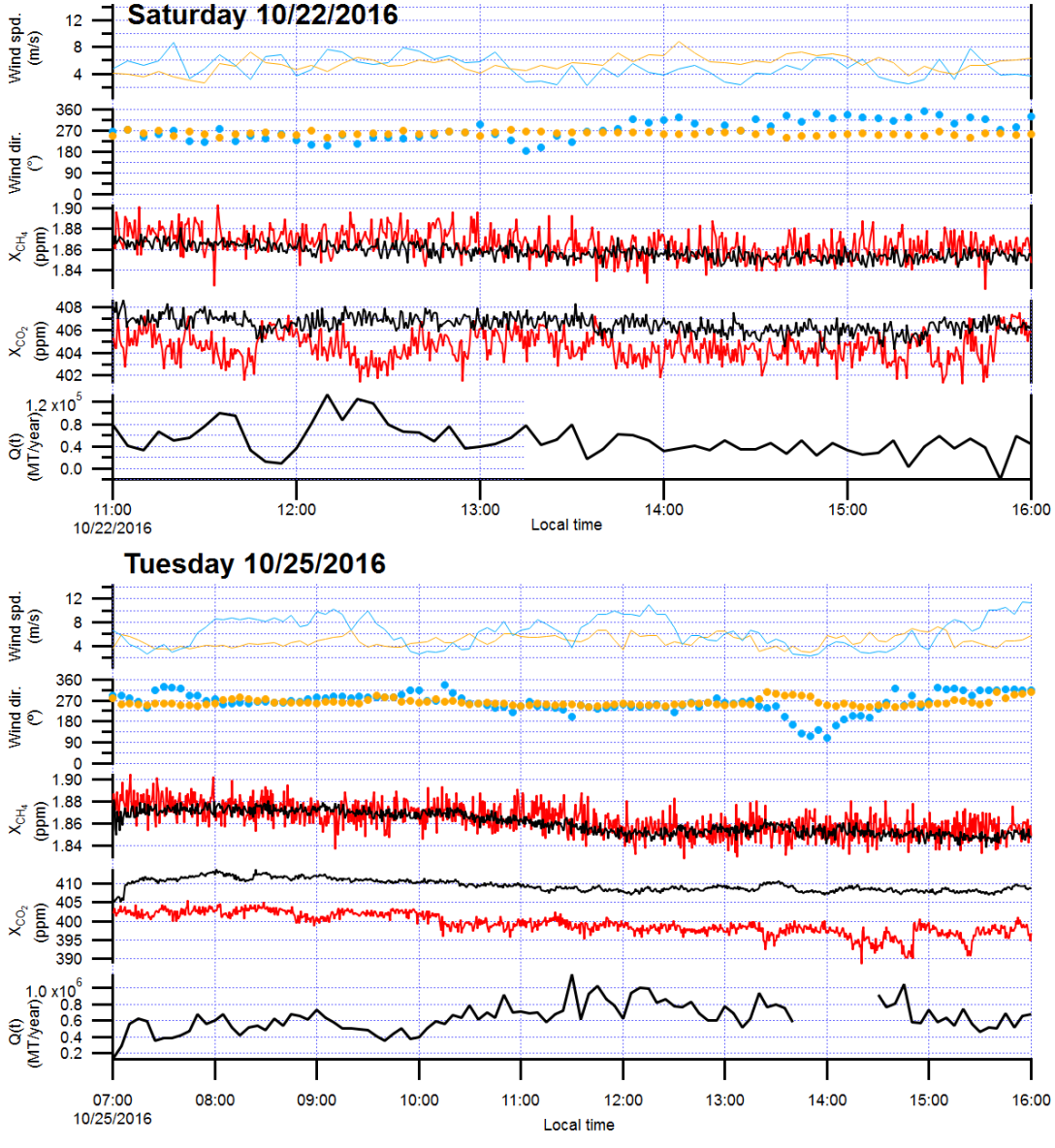

Figure 6: Time series data for the two case study days. Left plot: Saturday, 22 Oct. 2016. Right plot: Tuesday, 25 Oct. 2016. Figures show X_{CO2} and X_{CH4} over the reference path (red) and city path (black), as well as wind speed and wind direction measurements taken at NCAR Mesa (blue) and NCAR Foothills (orange). Bottom panel in each plot shows Q(t) for each day. On Oct. 25, Q(t) data near 14:00 has been removed since the reference path wind direction (NCAR Mesa) is out of the southeast to east, resulting in city contamination along the reference path.

692
693 Table I: Parameters used to calculate the emission rate from Eq. (4). The measurement precision refers
694 to the instrument uncertainty in the measurement quantity. The variability refers to the observed
695 environmental variability over the measurement period. The variability from the enhancement, the wind
696 direction, and the wind speed drive the observed variability in the estimated $Q(t)$. (The distance from
697 a given source location to the DCS measurement path, Δx_j , varies with location and has a 5-m
698 uncertainty.)
699

		10/22 11:00-16:00		10/25 10:00-16:00	
Quantity	Measurement precision	Mean	Variability	Mean	Variability
Pathlength L	0.15 m	6730.66 m	0	6730.66 m	0
Enhancement $(c-c_0)$	0.9 ppm (ref.) 0.5 ppm (city)	1.98 ppm	1.4 ppm (72%)	10.9 ppm	2.3 ppm (21%)
Wind speed u	0.3 m/s	5.2 m/s	0.85 m/s (16%)	5.6 m/s	1.4 m/s (25%)
Solar insolation	5%	570 W/m^2	76 W/m^2 (13%)	275 W/m^2	185 W/m^2 (67%)
Wind direction θ	2°	265°	20°	261°	27°

700